Experimental Results From Controlled Blade Tip/Shroud Rubs at Engine Speed

Corso Padova, Jeffery Barton, Michael Dunn, Steve Manwaring

Experimental Results From Controlled Blade Tip/Shroud Rubs at Engine Speed

Corso Padova

Jeffery Barton

Michael G. Dunn

Gas Turbine Laboratory,
Ohio State University,
2300 West Case Rd.,
Columbus, OH 43234

Steve Manwaring
GE Aircraft Engines,
Cincinnati, OH 45215

Experimental results obtained for an Inconel® compressor blade rubbing a steel casing at engine speed are described. Load cell, strain gauge, and accelerometer measurements are discussed and then applied to analyze the metal-on-metal interaction resulting from sudden incursions of varying severity, defined by incursion depths ranging from 13 μm t o 762 μm (0.0005 in. to 0.030 in.). The results presented describe the transient dynamics of rotor and casing vibro-impact response at engine operational speed similar to those experienced in flight. Force components at the blade tip in axial and circumferential directions for a rub of moderate incursion depth (140 μm) are compared to those for a severe rub (406 μm). Similar general trends of variation during the metal-to-metal con-tact are observed. However, in the nearly threefold higher incursion the maximum in-curred circumferential load increases significantly, while the maximum incurred axial load increases much less, demonstrating the non-linear nature of the rub phenomena. Concurrently, the stress magnification on the rubbing blade at root mid-chord, at tip leading edge, and at tip trailing edge is discussed. The results point to the possibility of failure occurring first at the airfoil trailing edge. Such a failure was in fact observed in the most severe rub obtained to date in the laboratory, consistent with field observations. Computational models to analyze the non-linear dynamic response of a rotating beam with periodic pulse loading at the free-end are currently under development and are noted.

1 Introduction

Contemporary gas turbines rely on complex blade-casing rub-in-systems to improve the tip clearance behavior during operation from initial service to maximum lifetime [1,2]. Higher energy efficiency is achieved by reducing tip clearance between the rotor and the stationary casing components, but as the clearance is reduced, the probability of a rub occurring during some operating conditions also increases. Blade-to-case rubs can degrade the operation of an engine through the induction of high-amplitude shaft vibration and severe blade/seal wear, and may lead to catastrophic failure of the engine in the worst occurrence.

Advances in the prediction of the complex dynamic of vibro-impact systems with multiple degrees of freedom are currently needed to enable the formulation of a comprehensive design methodology for rub-in systems, particularly one capable of predicting and taking advantage of the potential offered by new and emerging rotor/blade concepts. This need is driving studies based on recently acquired experimental capabilities such as the one reported in this paper as well as computational studies that analyze the non-linear dynamic response of blades under periodic pulse loading [3,4].

In combination with continuing progress in other more mature allied technologies, such as rotor dynamics under severe disturbances [5–7], forced vibrations of bladed disks [8,9], and abradability of materials [10], the improved understanding of the phenomena that affect blade-casing interactions is expected to result in savings in gas turbine maintenance costs applicable not only in propulsion engines but for stationary advanced power systems as well.

2 Experimental Method

The development of an in-ground spin-pit facility (SPF) capable of rotating at engine speed and specifically designed to investigate aeromechanic phenomena for gas turbine engine hardware was recently reported [11]. The underground containment tank that houses both the rotating component and part of a high-stiffness spindle is cylindrical (1.52 m in diameter by 0.65 m high), and has 0.90-m-diameter openings at the top and at the bottom.

Vertical axis spin testing for design validation of turbomachinery components dates back to World War II applications, which sought to solve problems with military aircraft turbochargers. However, the research interest envisioned from the inception of this facility design dictated the use of a high-stiffness spindle. This requirement forced a significant departure from the common way of performing a spin experiment, whereby a rotor is suspended in the heavily armored vacuum tank from a flexible shaft. That shaft arrangement allows the rotor to find its own balance axis and eliminates the need for extreme precision in mounting and balancing. Unfortunately, it is unsuitable to reproduce blade-to-case rub situations for which one wishes to derive physics based modeling of the events occurring at the blade tip/casing interface.

Thus, a major subsystem component required for the facility is a vertical and high-stiffness spindle capable of operating at 20,000 rpm for a reasonable period of time. The system utilized here incorporates hybrid bearings and an oil mist lubrication system. The spindle shaft is driven from the top by an air turbine motor. The single-stage engine rotor is bolted beneath the spindle assembly and is surrounded by the containment test chamber. The first critical speed of the spindle is significantly higher than the maximum operating speed. The analysis of the high-stiffness bearing arrangement indicates a shaft critical speed of 23,500 rpm for the design manufacturing tolerances and assumed operating temperature effects. This component was described in full detail in Ref. [11].

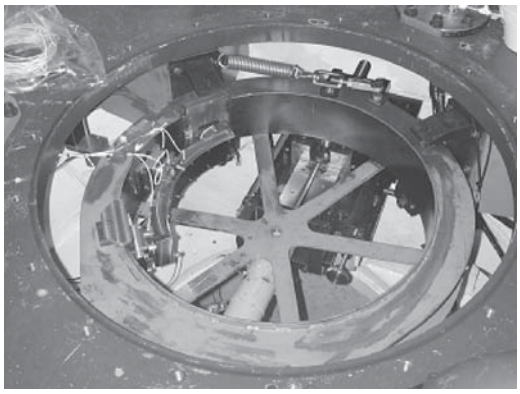

Fig. 1 Incursion mechanism photo

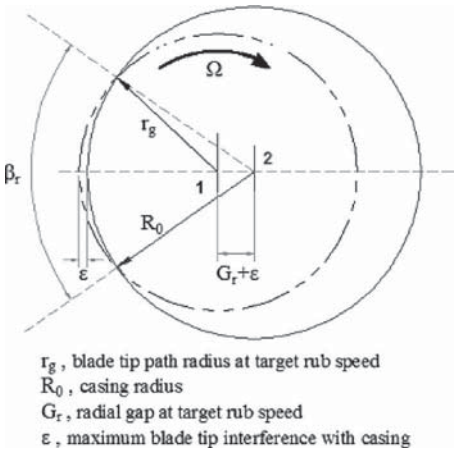

Fig. 2 Rub geometry

A second major subsystem required to investigate blade-to-case rubs is a fast-acting mechanism that allows insertion of the engine casing into the path of the bladed rotor under conditions for which the pre-set interference between the casing and the blade can be controlled to within less than 13 μm (0.0005 in.). Such a mechanism was designed and developed to research asymmetric and full rotor clearance closure for engine stages. For single-blade asymmetric clearance closure investigations, a rapid contact of the bladed rotor with its housing is simulated as would occur in an abrupt flight maneuver. For full rotor clearance closure, an extended contact of the bladed rotor with its housing is simulated as could be experienced in some flight phases due to temporary thermal imbalances in different parts of the engine. The known requirements for those types of investigations have defined the general layout of the electromechanical, pneumatic, and measurement subsystems of the facility. The fast-acting incursion mechanism is briefly reviewed below, but was described in full detail in Ref. [11].

The function of the incursion mechanism is to move the engine-case segment into the blade path at an exact time for a precise distance and duration, which determines the number of blade strikes. After a few strikes, the mechanism retracts the casing out of the blade path. The disk containing the blade is operating at engine speed and may contain a single airfoil or multiple airfoils. In the current configuration, a 90 deg sector of a representative engine casing is forced to rub the tip of a single bladed compressor disk for a limited number of times with pre-determined blade incursion into the casing. For the measurements described herein, the speed at the time of rub was on the order of 17,000 rpm. For this rotational speed, the instrumented airfoil returns to the same circumferential position in 3.8 ms; thus, several contacts between blade and shroud are experienced before the eccentricity disturbance is removed.

The compressor disk and blade rotate on a vertical rigid spindle that is driven by an air turbine. The casing sector is mounted on a rigid transfer bar that is backed by three piezoelectric load cells and this assembly (load measuring unit, LMU) is attached to a support ring that swivels in the horizontal plane. A single throw fast acting gas operated piston is attached to a cam follower that is rigidly connected to the support ring and activation of the piston moves the casing in and out of the path of the rotating blade over a time interval of about 20 ms. The incursion of the rubs is prescribed by setting the initial position of the mechanism in increments of 5 μm (0.0002 in.). Figure 1 shows a picture of the subsystem.

2.1 Rub Geometry. The interference between blade tip path and engine casing in ramp-incursion experiments is simply described by Fig. 2. The maximum incursion depends on the initial gap and the eccentricity that is commanded between the casing circle and the spindle axis. For a wide range of interference values, a 90 deg sector of the casing was found sufficient to obtain rubs of significant depth. A similar rub geometry was investigated a few years ago by Ahrens and others [12,13] to derive contact forces during blade rubbing. However, the rotational speed of the blade was 1800 rpm, nearly an order of magnitude smaller than in the experiments that are reported here. In addition, the airfoil consisted of a simple beam of rectangular cross section.

From Fig. 2, consider that a blade of outer radius r_0 is mounted on a disk with center on the spindle axis (point 1). Initially, the casing with larger radius R_0 also has its center on the spindle axis, thus resulting in a clearance G_0. When the rotor is accelerated to an angular velocity Ω, the disk and the blade are subjected to a centripetal force field that moves the blade tip to an outer radius r_g, resulting in a new clearance G_r at the target rub speed.

At the target rotational rub speed, the incursion mechanism commands a displacement of the casing circle equal to $(G_r+\varepsilon)$, where ε is the maximum desired interference for a rub. As a result the casing circle with radius R_0 is now centered away from the spindle axis at point 2 in Fig. 2 and the blade incurs an interference varying from 0 to ε and back to 0 along arc β_r. The angular length of the rub is easily obtained from Fig. 2 as

$$\beta_r = 2\arccos\{(R_0^2 + (G_r+\varepsilon)^2 - r_g^2)/[2R_0(G_r+\varepsilon)]\}$$

In preparation for the metal-on-metal rubs described in this paper, the precise variation of G_r with angular velocity was established experimentally. This was done by first setting a known eccentricity between the casing support ring and the rotor and then bringing the spindle gradually up in speed until a very light touch of the blade was obtained. By repeating the process for several values of the initial eccentricity the gap calibration curve was obtained.

2.2 Instrumentation. The SPF is designed to accept fast response sensors installed both on the rotating disk/blade assembly and on the stationary casing sector or load measuring unit. The shaft of the spindle is hollow and accommodates the bundle of wires from several blade-mounted strain gauges or surface bonded precision resistance temperature devices. For the experiments discussed here, the airfoil was instrumented with miniature dynamic strain gauges arranged on the suction and pressure side of the blade. Eight unidirectional gauges and four rosette gauges were installed. The blade had been fully characterized during compressor development by measurements using multiple strain gauges during excitation by a pulsating air jet. The results from those experiments were used to select a subset of gauge locations best suited to analyze the blade vibratory response during rubs. Excitation power and signal response are carried by electrical wires routed through the spindle to the rotating terminal of a 200-channel slip ring unit. The stationary terminal of the unit is di-

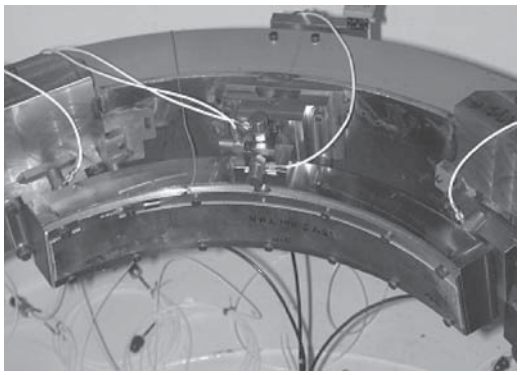

Fig. 3 Load measuring unit (LMU)

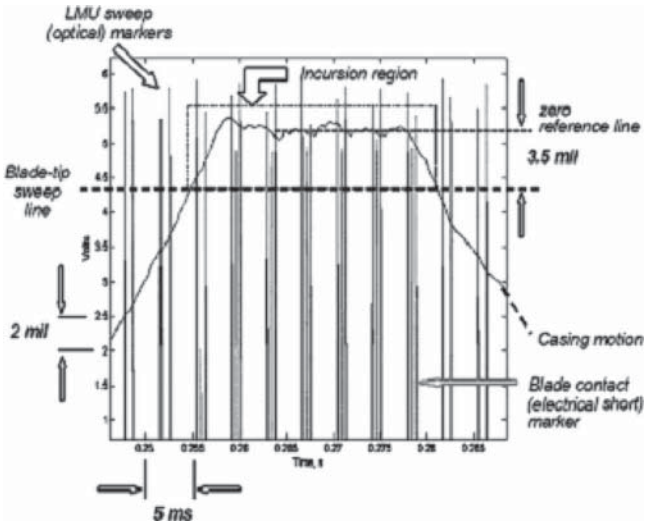

Fig. 4 Casing motion and incursion region

rectly patched into the high-speed data acquisition system. All strain gauges were operated in constant current mode for the present experiments.

The stationary casing (or LMU) is instrumented to measure forces and moments. The segment of engine casing against which the blade rubs is carried by a metric support that includes three load cells. Each piezoelectric load cell measures three force components. Two end cells are placed below the load line, which is located in the mid-plane of the engine case. The center cell is located above mid plane. The arrangement of this LMU is thus designed to minimize the moment loads on each cell and to obtain moment information about three mutually perpendicular axes.

Five accelerometers are also mounted on the LMU, which is shown in Fig. 3. Three radial directions are measured at locations very close to each load cell. A triaxial block, which is mounted near the center load cell, is equipped with the remaining two accelerometers that measure one axial and one circumferential direction in the middle of the LMU.

The dynamic response of the entire LMU was investigated to correctly relate the intensity and frequency of the excitation rub forces to the load cell measurements. The frequency response of an individual piezoelectric load cell is an important parameter. The Kistler Type 9047B sensor selected for the LMU is characterized by high rigidity ($K_x = K_y = 700$ N/μm; $K_z = 6000$ N/μm) and thus has a high natural frequency ($f_0 = 120$ kHz).

The load cell shows relatively little vibration damping at the upper frequency limit. Frequencies can be triggered up to about a third of the natural frequency with very small measuring errors. The lower frequency limit is determined by the drift of the charge amplifier and the quality of the insulation. For the very short measuring times of interest in this application, measurement errors at low frequencies are very small.

A next step in characterizing the dynamic response of the LMU was taken by carefully observing the force response in repeated measurements while applying the same impulsive excitation force with a modal hammer. The observations were then matched with the predictions of a simple one degree of freedom model for the locally dominant mass, stiffness, and damping characteristics. The model indicates the following values for the system parameters

$m = 4.0$ kg (8.81 lb), equal to 49% of the total LMU mass mounted forward of the load cells

$k = 400$ N/μm (2.284 M lbf/in.), equal to 6.7% of the nominal z-direction load cell rigidity

$\zeta = 0.0433$, damping ratio

For such a model, the underdamped vibrations occur at a frequency of 1069.8 Hz (the natural frequency of the system is 1611.3 Hz) and a logarithmic decrement $\delta = 0.272$. This oscillation matches the experimentally observed response over a few periods after the initial transient lasting about 0.75 ms (about 2.68 times the duration of the excitation impulse).

Additional considerations on the investigations of LMU dynamic response are discussed later in the data analysis section.

2.3 Data Acquisition. During a typical experiment, the rotor is accelerated to the target speed in less than 3 min. As the rotor speed approaches the target value selected for a rub to occur, the angular acceleration is gradually decreased so that the airfoil impact with the shoe occurs at a constant rotational speed. For all the experiments presented, the rotational speed at impact was held at 15,990 rpm. A few rubs of the single blade installed onto the bladed disk are then obtained as described in the following paragraphs.

First, the casing movement toward the spinning blade tip is initiated by the triggering system described later in this section. This results in the casing motion shown in Fig. 4 in the initial region of the abscissa (time axis). Each division of the ordinate represents a 2 mil displacement of the casing toward the spinning blade that is located at the top of the figure. Also shown in the figure are the vertical markers that indicate the arrival of the blade at the entrance of the casing sector and the departure of the blade from the casing sector. At a rotational speed of 15,990 rpm the duration of one sweep of the single blade in the disk over the casing sector is about 1 ms. Eleven blade sweeps are shown in the time span given in Fig. 4 (see LMU sweep legend). As the blade passes over the LMU in the initial region of the time axis, there is sufficient clearance between the blade tip and the shroud to avoid a rub.

Second, during the casing motion, the tip sweep line is crossed as depicted in the figure. After this point in time, the LMU is in the path of the spinning blade and a rub is obtained as soon as the blade returns over the LMU sector. This is shown by the appearance of the blade contact marker in the figure. The duration of blade/shroud contact is generally less that the blade sweep duration and depends on the prescribed incursion depth. Except for a range of very small incursions, the rubs begin with the casing still advancing toward the spinning blade. For more severe incursions, more rubs occur before the casing locks into the zero-lead segment of the casing movement (maximum incursion position). The zero-lead incursion duration is clearly indicated in Fig. 4 by the plateau in the casing movement trace and is labeled "zero reference line."

Third, during the time that the casing is in the maximum incursion position, up to six rubs can take place for the values of

rotational speed at which experiments were conducted. Due to the settings chosen in the triggering circuit, five rubs were obtained in most cases. All zero-lead incursions occur with the same nominal interference between the path of the blade tip and the arc of the casing. The deviation of the actual interference from the nominal value was monitored in repeated experiments and found to be less than ±3.8 μm.

Fourth, the continuing motion of the cam forces the casing to begin to retreat. In this phase, the rubs continue because the casing is still inside the incursion region. As before, the more severe the incursion, the more rubs occur before the casing clears the exit boundary of the incursion region.

Finally, the casing crosses the tip sweep line and the rubs end. In the experiments discussed below, the maximum incursion imposed was for 406 μm and resulted in a total of 15 rubs.

The trigger to start both the data acquisition and incursion systems must be precisely controlled. The high-frequency data acquisition system has a selectable window in which to collect data and record the rub events, and must be triggered at the appropriate moment. The individual measurement channels are sampled simultaneously at a rate of 100 Khz using the 12-bit data acquisition system. The triggering circuitry for the ramp-incursion experiments is fairly involved. The object is to get the casing sector to move out and set in place during the time interval when the blade cannot interfere with the casing surface. This time interval spans several blade revolutions, as can be seen from Fig. 4. Using a selectable time delay from a trigger that is related to instantaneous blade position, the objective is achieved by delay increments equal to a fraction of one revolution. An optical sensor placed to sense arrival of the blade at the leading edge of the casing supplies the trigger signal. The incursion system timer can resolve to a millisecond, which is too coarse for this application, so a delay generator capable of resolving to 0.1 ms is placed in front. A manual trigger-enable switch disables the sensor trigger until the rotor set speed is achieved.

The data acquisition system is triggered with the incursion system timer so that casing movement can be monitored during the experiment and correct position relative to blade location can be verified. In each experiment, the data acquisition system is always running in sample-and-hold mode after a manual enable command, and a pre-rub hold time is programmed into the system. Thus any of the measurement histories show typically a pre-rub value for about 200 ms followed by the rub event sequence. Typical histories last 410 ms to 829 ms and consist of a few to several rubs depending on the preset incursion depth and the type of experiment.

3 Data Analysis

The measurements obtained simultaneously from load cells, accelerometers and strain gauges during nearly a second of data acquisition time, when combined, offer a detailed description of the rub phenomena. The purpose of this paper is to describe the results from rubs of an Inconel® compressor blade on a bare steel casing. We do have data for the same blade rubbing on different coatings, but introduction of that material is beyond the scope of this paper. Extensive results from specific applications and research projects on the effect of casing coatings on rub dynamics will be the subject of subsequent papers. In this section load cell, strain gauge and accelerometer measurements are first reviewed qualitatively and then applied to analyze the metal-on-metal interactions.

3.1 Measurements Overview. Typical measurement time histories are shown in Figs. 5 and 6. In these figures, the initial pre-rub level of the sensor signal, the response during multiple rubs, and the post-rub sensor signal are easily identified.

The three load cell measurements from top to bottom of Fig. 5 are for the initial cell, center cell, and last cell passed by the blade during each revolution. Note how quickly after the rub interval the measured loads return to the pre-rub level.

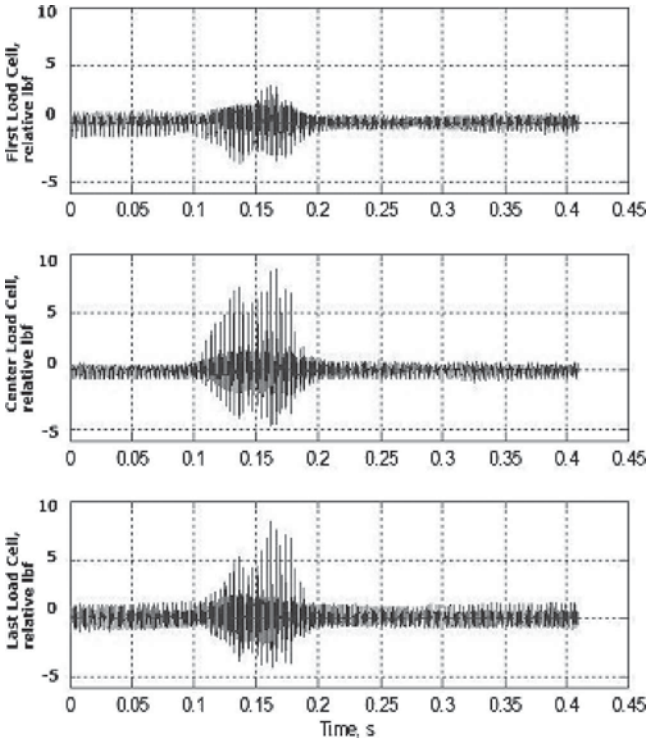

Fig. 5 Typical load cell measurements

The measurements of acceleration are qualitatively very similar to those obtained from the load cells.

The two typical strain gauge measurements from top to bottom of Fig. 6 are for a gauge located at the tip and for a gauge located at the root of the blade, respectively. Note that the tip gauge indicates localized disturbances during the rubs, a displacement of the baseline that is believed to be a temperature-induced, and no post-rub oscillations. In contrast, the root gauge shows oscillations building up from rub to rub followed by an exponential decay after the last rub, but does not show a baseline offset.

3.2 Rub Conditions. It is important to note that the measurements obtained during each experiment should be examined according to a number of different time scales. Five scales are illustrated in Fig. 7. In order of decreasing duration they are: the time

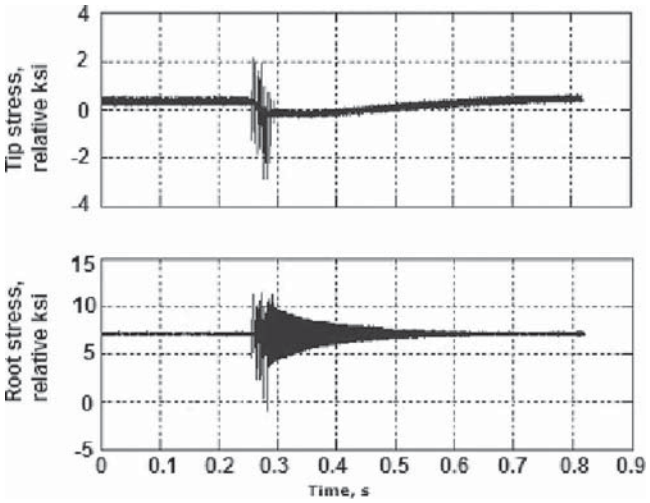

Fig. 6 Typical strain gauge measurements

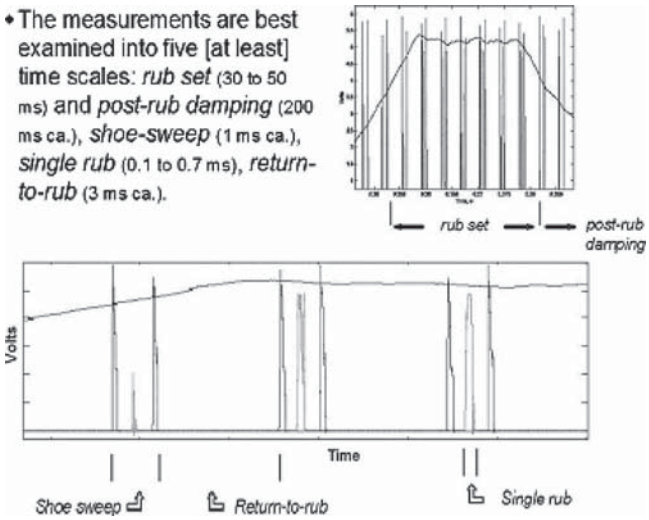

Fig. 7 Time-scales of blade rubs

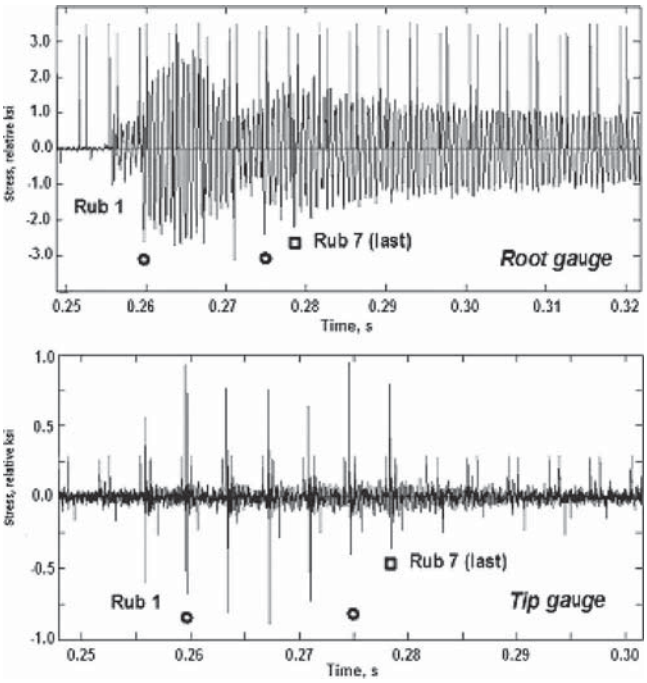

Fig. 8 Strain gauge measurements for rub-set and post-rub damping time scales. Incursion: ε=89 μm (0.0035 in.).

of damping of blade excitation after a set of rubs, the time spanned by an entire set of rubs, the time for one casing (shoe) sweep, the time interval a blade spends in free oscillation after a rub and before returning for a subsequent rub, and the duration of an individual rub. The first two scales are shown in the top part of the figure. The bottom part of the figure zooms in on three distinct blade rubs and shows the three remaining time scales.

The two types of markers discussed earlier are recorded during an experiment to identify the different scales of the rub phenomena. The optical blade-passage markers unequivocally identify the time interval for potential contact and the angular velocity, the electrical blade-contact signal registers actual strikes. In each experiment, the data acquisition system is already running in sample-and-hold mode at the precise instant when the command to acquire measurements is received, and a pre-rub hold time is programmed into the data system. Thus any of the measurement histories shows typically a pre-rub value for about 200 ms, the onset of the rub event, the dynamic response resulting from the impact of the airfoil with the shoe, the release of the airfoil immediately following detachment from the shoe, the vibrational response of the airfoil as it rotates around once more after having been initially excited by the impact, the effect of repeated impacts, and the decay in dynamic response after the conditions causing the incursion have been removed.

One might ask how the above sequence of events is related to rub occurrences in flight. It is clear that in the experiments just like in flight, for a given incursion depth or severity of a rub event, the rate of incursion in each strike will be positive, null or negative during different phases of the set of rubs that makes up an event. By comparing measurements across variables, the effects of incursion depth and rate of incursion can be separated. One way in which the experimental results shown herein differ from the flight situation is that the initial temperature of the components is room temperature and is not elevated as it would be in flight. That difference will be removed in subsequent measurements.

3.3 Vibrations and Loads in Multiple Rubs. The effects of rub repetition can be identified using the measurements presented here. For the example shown above, the first rub is clearly a partial incursion and is followed by rubs of equal duration (250 μs). However, the first rub is important although not a full engagement, because it is this rub that causes the initial vibratory response of the airfoil. In addition, in zero-lead rubs, the deviation of the actual interference from the nominal value was monitored in repeated experiments and found to be less than ±3.8 μm (±.00015 in.). Rubs 2 and 3 are equal in duration and incursion depth. However, as the blade comes around after each rub, it is excited and one would intuitively expect that rubs 2 and 3 will be different in blade vibratory response and in tip loads during contact to the casing. The extent to which this was found to be true is shown in the results that follow.

First we turn to the topic of overall blade/casing response during an entire rub-set and beyond. Figure 8 shows the alternating stresses versus time, on the top is the root strain gauge, and on the bottom is the tip strain gauge. The vertical markers identify the time intervals during which the blade sweeps over the LMU. As shown earlier, during a fraction of this time the blade comes into contact with the casing surface: a strike occurs and this strike may include an initial hit, partial or full detachment, and subsequent hits. Note the different scales on the vertical axes for the root and tip gauge. Also note that the markers have been arbitrarily scaled in the measured voltage for the sole purpose of visualizing the LMU sweeps.

In this rub event (there were seven strikes in total), each of the strikes is identified by labels, numbers, and symbols: the first strike is labeled and the seventh strike is marked with a square symbol, the first and last of all zero-lead strikes (strike numbers 2 to 6) are marked with round symbols. The first strike occurred with an incursion depth of 51 μm (0.002 in.) and an incursion rate estimated at 1 in./s as the casing is advancing into the blade. All zero-lead strikes are at a nominal incursion 89 μm (0.0035 in.). The seventh strike occurred with an incursion depth of 76 μm (0.003 in.) and a negative incursion rate (casing is retreating away from the blade) of 3.8 m/s (1.5 in./s).

Following the root strain gauge measurement in more detail, strike 1 is not a full engagement, but it excites some vibration modes of the blade. This initial rub is followed by several of the zero-lead rubs, all nominally equal in incursion. Yet an uneven progression of alternating stresses results, first increasing then decreasing, then increasing again. This is interpreted as being an effect of different boundary constraints in repeated strikes due to the conical geometry of the casing, the unwrapping motion of the blade and phase differences in the oscillations of the blade as it returns to interact with the casing. After strike 7, stresses decay

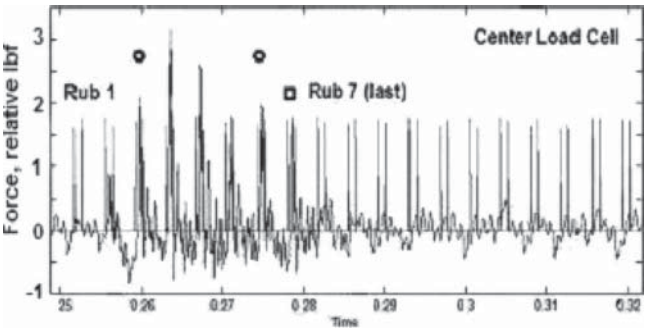

Fig. 9 Center load cell measurement for rub-set time scale. Incursion: ε=89 μm (0.0035 in.).

gradually.

Following the tip measurement in detail, only stress spikes induced by the contact loads are observed. The magnitude of the maxima and minima of stress are indicative of changing boundary conditions of the blade as it returns to interact with the casing. It is also possible that a portion of the observed activity may be the result of the interaction between natural and forced vibration frequencies of the airfoil. Details of the tip loads and waveforms will be discussed later in this section.

Figure 9 shows the load measurement at the center location of the LMU. The peak loads registered in strikes 1 and 7 are consistent with the expectation based on incursion and incursion rate conditions. The peak loads registered in the five zero-lead strikes match the trend shown by blade stresses: increasing load in strikes 2 and 3, decreasing in 3, 4, 5, and the increasing again from 5 to 6.

Moderate variations in the pattern described above for the root alternating stresses were observed as the incursion depth increased from 13 to 406 μm (0.0005 in. to 0.016 in.). Specifically, minor variations were noted in experiments 22, 23, and 24. The pattern changes more markedly in going from incursion depth of 89 μm to 140 μm (0.0035 in. to 0.0055 in.) and above. By contrast, a progressive increase in the measured peak loads was observed as the incursion depth increased from 13 μm to 406 μm (0.0005 in. to 0.016 in.).

3.4 Vibrations and Loads in a Single Rub. Returning to the overview of the shoe-sweep time scale, it is instructive to compare one of the zero-lead rubs, i.e., number 3, to the first rub. Figure 10 shows the data for the root gauge and the tip gauge on an expanded time scale. It is noticeable that the time histories show distinct spikes at the beginning and end of the most perturbed region. The time interval between these two spikes correlates well in all experiments with the indications of electrical contact shown earlier as the blade-contact marker, so the first spike is taken as indicating an attachment stress wave and the last spike a detachment stress wave. In this case the blade contact lasted about 200 μs.

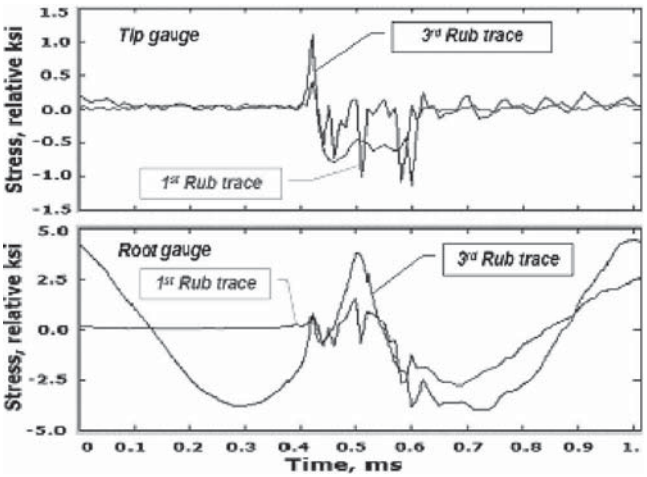

Fig. 10 Strain gauge measurements for shoe-sweep time scale. Incursion: ε=140 μm (0.0055 in.).

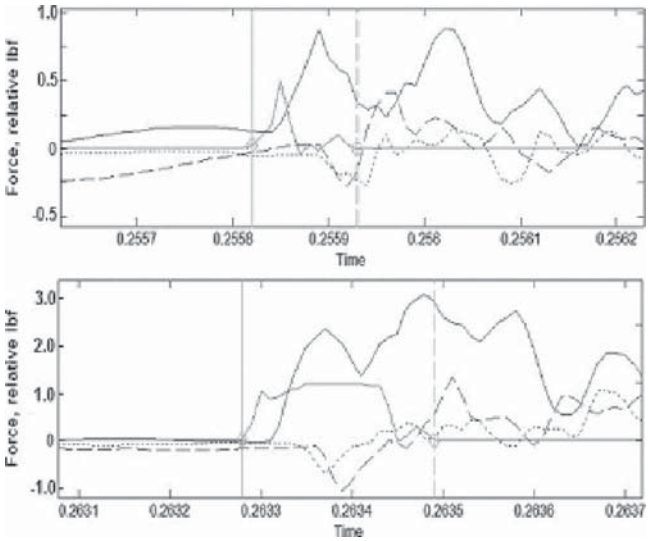

Fig. 11 Load cells measurements for shoe-sweep time scale (first rub: top; third rub: bottom). Incursion: ε=89 μm (0.0035 in.).

It must be stressed that these times are consistent with the durations involved in a real engine rub. It is necessary to understand the physics under these conditions for real engines, not at some longer duration that is easier to obtain experimentally.

Looking first at the root gauge, the first rub is not a full engagement rub. The centrifugal load has been subtracted out and we see that relative stress is zero up to the first attachment. There is some high frequency content probably related to a changing area of contact as the airfoil flexes and twists under load, and after a low-frequency oscillation gradually develops. It is a first flex frequency that persists also at later times. The detachment spike is visible. Notice that it is a bit early relative to the companion event in the third rub. Again, this is not a full engagement strike.

Now let us follow the third rub. The blade comes around and is excited in the first flex mode. The blade attaches first and the resulting history is more suggestive of an increasing-decreasing contact area. The blade then detaches and resumes the first flex motion.

Looking now at the tip, the following occurs: the start of the first rub contact is clearly marked by a first positive spike followed by smaller disturbances because of varying contact area and local blade detachment. A marked negative spike marks final blade detachment. In the third rub the spike marking the initial blade impact is stronger followed by a more uniform load during contact consistent with a deeper incursion. The detachment spike again ends the strike at about the same level encountered during the first rub.

It is now of interest to extend the above overview of the shoe-sweep time scale to the load cell measurements. Figure 11 shows the time histories for the first rub and the third rubs (the second of the zero-lead rubs). In the top frame of Fig. 11, four lines are shown: one line is the record of the electrical blade contact, the three other lines are loads measured from the LMU entrance cell (dotted line), the center cell (solid line), has ordinates above zero only between the vertical marker lines and the exit cell (dashed line). The figure is for the first rub, when the blade makes contact

to the casing just a short distance prior to passing the center load cell. It is seen that the center cell responds immediately measuring a positive load while the entrance and exit cells respond with some delay and a negative load at first. A first bending mode LMU displacement is consistent with these measurements.

The bottom frame of Fig. 11 shows similar histories for the third rub. The general trend observed above is still valid but the increased load levels associated with a deeper and sustained incursion (as evidenced by the solid line for the center cell) are also apparent.

Clearly, even in this very preliminary look at the measurements, purely based on an initial survey of the time-series measurements, one can follow a lot of the physics of rubs at a relevant engine speed. Some fundamental aspects of the phenomena are also well recorded.

3.5 Measurements Processing. As demonstrated by these results, rub phenomena occurring at rub speeds consistent with engine operation are indeed very complex. It is very useful to describe and interpret these results after extensive processing in the frequency domain. To this end, the results that are reported and discussed in the next section have been obtained by applying fast Fourier transform techniques at two levels.

First, for the strain gauge measurements the power spectrum density (PSD) of each signal was obtained and segmented in three relevant frequency domains in order to compare spectral magnitudes to the known blade natural frequencies. Those frequencies were available experimentally from routine compressor qualification tests. The aim at this stage of interpretation of the rub experiments was to identify stress intensification factors during rubs at the natural frequencies or elsewhere in the frequency domain for design purpose. Results from these analyses will be discussed in the next section.

Second, for the load cell measurements, a matrix of frequency response functions (FRF matrix) for known input loads onto the casing surface was generated in pre-experiment broadband modal tests of the LMU. Processing of the load cell signals after the experiments using the inverse of the FRF matrix and the known blade location results in reconstruction of blade tip loads. Currently the algorithms for load cell processing are satisfactory only up to 8 kHz, a frequency cutoff incurred by the application of the reference input loads while using the modal hammer. In principle, that limitation can be removed by a process of PSD averaging over multiple traces. However, that remains to be implemented and signal-to-noise limitations could still limit the accuracy of the process. At the same time narrowband modal testing using a piezoelectric shaker and finite-element modeling of the entire LMU structure are in progress. These steps can be combined and are expected to circumvent the inherent difficulty raised by measuring rub events; namely, the excitation of a wide range of vibrations of the experimental rig due to the high-frequency components in the contact forces. Clearly, excitation of the natural frequencies of the LMU and support structure leads to an amplitude and phase distortion in the load cell measurements that must be properly accounted for in the final data reduction algorithm.

4 Results and Discussion

4.1 Post-Rub Photographs. At this stage in the research, only still photography executed after each experiment has been deployed to document casing and blade conditions following several rub strikes. High speed imaging of the blade deformations during, between, and immediately after successive casing strikes will be available in the near future.

A few photographic records from the growth and ramp-incursion experiments with a single blade on the disk impacting on metal casing are shown in Figs. 12–15. The simple technique of spraying a light coating of machinist blue ink on the metal casing surface before each experiment was sufficient to successfully visualize the location and extent of blade tip contact to the engine casing sector. The method is readily implemented and effective to visualize even grazing rubs, having incursions well below the LMU motion resolution of 5 μm (0.0002 in.). At the most severe incursion investigated to date, this simple method has also recorded the interesting oscillatory pattern of the tip of the blade due to torsional excitation. The obvious drawback of post-experiment photography is that is presents an integrated record of multiple strikes, thus driving one towards instantaneous imaging.

Fig. 12 Blade and casing after very light rub

Figure 12 shows the blade and casing after a very light rub. Pre-test predictions indicated that the combined axial, radial, and circumferential deformation of the airfoil would result in the tip surface coming into contact with the conical casing surface at a location mid-rear chord. The prediction was verified by the experiment. The angular length of the rub was measured at 8 deg, also as predicted by the geometry considerations given earlier.

Figure 13 shows a closeup of the trailing edge of the blade. Under the rub conditions accumulated on this blade there were no signs of plastic deformation or significant burrs at the tip. The discoloration of the epoxy used in bonding and coating the strain gauges is the only indication of the severity of the conditions encountered by the blade. A local instantaneous temperature above 160°F would result in the clear epoxy change in color according to the manufacturer.

Figure 14 shows the casing after experiment 30, for an incursion at 406 μm (0.016 in.) of the single blade rotating at 15,990 rpm. Here, too, the airfoil did not sustain significant damage. The angular extent of rub was measured at 52 deg.

In contrast, Fig. 15(*a*) shows a closeup of the airfoil after experiment 31, where an impact incursion at 762 μm (0.030 in.) was sustained by the single blade rotating at high speed. There is significant plastic deformation of the overall airfoil shape, a removed portion at the trailing edge tip, as well as definite local

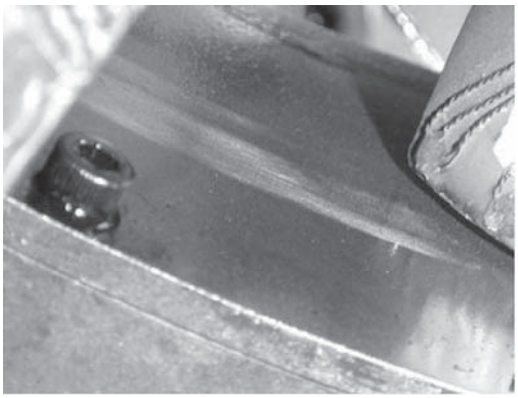

Fig. 13 Closeup of blade trailing edge and casing after several moderately light rub experiments

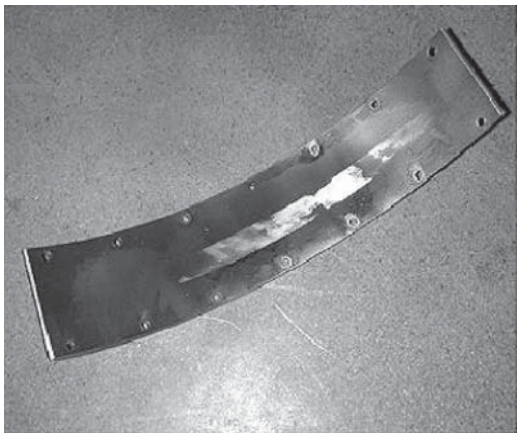

Fig. 14 Casing after rub of experiment no. 30. Incursion: ε =406 μm (0.0160 in.).

damage along the leading edge of the blade. The concomitant rub swath recorded on the casing by the removal of the ink is shown in Fig. 15(*b*). The pattern that is revealed by alternating light and dark areas is consistent with a strong torsional oscillation resulting in alternating high surface stresses toward the leading edge and trailing edge of the tip.

(*a*)

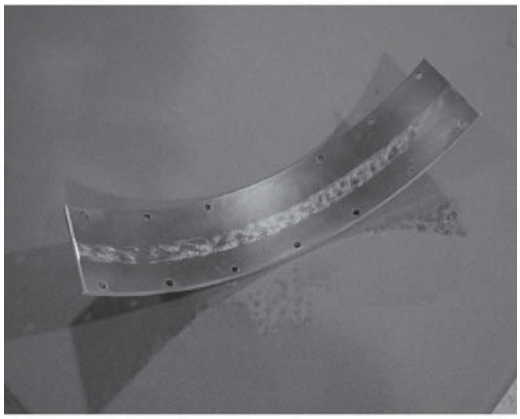

(*b*)

Fig. 15 (*a*) Closeup of blade after experiment No. 31. Impact incursion at ε=762 μm (0.0300 in.). (*b*) Casing after rub of experiment No. 31. Impact incursion at ε=762 μm (0.0300 in.).

4.2 Tip Loads. Results of tip loads will be presented and discussed next. These loads were obtained from the time series of load cell measurements shown earlier as follows.

During a rub experiment, nine response measurements are recorded from an unknown force at the rub surface. It is precisely this resultant force that is computed from the known instantaneous blade position and from the inverse of the output FRF operating on the load cell measurements transformed to the frequency domain. The computation above is then repeated for a discrete set of blade positions during the rub.

At present, issues associated with the detailed requirements of impulse vibration testing have restricted the application of the FRF algorithm to two components of the blade tip load, the axial and the circumferential component. However, finite element structural modeling is in progress to remove such a restriction. In the meantime, even with the restriction to two components, interesting comparisons of tip loads have been obtained, as illustrated below.

Even with the above restrictions, the tip loads indications are very interesting. Figure 16 shows results from the 140 μm (0.0055 in.) incursion (experiment # 26). The axial tip load derived in each of the eight strikes incurred during the experiment is shown in Fig. 16(*a*). The spacing of the data points indicates the angular resolution associated with the processing of the load cell measurements for several airfoil locations. At the rotational speed of 15,990 rpm, a time interval of 100 μs corresponds to about 10 deg rotation. The first two rubs of the single blade installed on the bladed disk are for advancing casing and show axial forces considerably lower than the remaining rubs. In all zero-lead rubs, the maximum axial load is established quickly at the beginning of the event and decreases gradually during the rub. This may result from a relatively large deformation of the airfoil more than compensating for the trend in incursion depth shown earlier in the rub geometry section of this paper. The results for circumferential tip loads are shown in Fig. 16(*b*).

The axial and circumferential tip loads derived in each of the five zero-lead strikes incurred during experiment no. 30 [maximum incursion depth of 406 μm (0.016 in.)] are shown in Fig. 17.

The same general trends are noticed even as the incursion depth of the rub has increased threefold. However, it is interesting to note that while the maximum incurred circumferential load has increased 53%, the maximum incurred axial load has increased only 12%. These results underscore emphatically the highly nonlinear nature of the rub phenomena.

4.3 Blade Vibrations and Stresses. The blade vibratory response was analyzed with the primary objective of deriving design guidelines regarding significant changes in excited frequencies, modal shapes, and stress magnification during rub events. During compressor design, it is industry practice to thoroughly investigate airfoils to identify their dynamic characteristics by analytical methods and testing. Finite-element analysis and experimental techniques are routinely applied to locate the natural frequencies of the blade and to provide information on the modal shapes.

The blade used in the OSU experiments had been fully characterized prior to the rub measurements by finite elements calculations and by measurements using multiple strain gauges during excitation by a pulsating air jet. The air jet was operated at a frequency range of 0–31 kHz, and the responses of the blade were measured. Alternating stresses at discrete frequencies and blade locations on both suction and pressure sides identified mode shapes and natural frequencies of the blade from maximum stress location and stress distribution in nearby gauges. The data from the strain gauges at each natural frequency (1.4, 4, 4.7 kHz,…) identified were available prior to the OSU experiments in a normalized format (percent of maximum value) like that shown, for example, in Table 1.

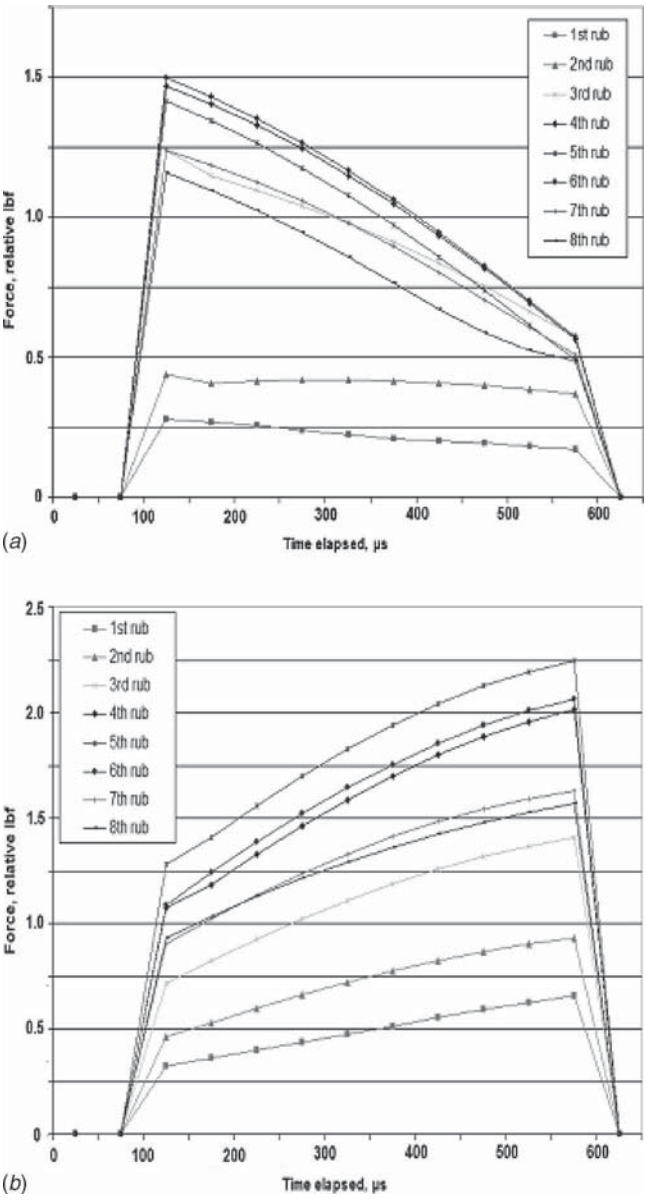

Fig. 16 (*a*) Axial component of tip force on airfoil in experiment no. 26. Incursion: ε=140 μm (0.0055 in.). (*b*) Circumferential component of tip force in experiment no. 26. Incursion: ε=140 μm (0.0055 in.).

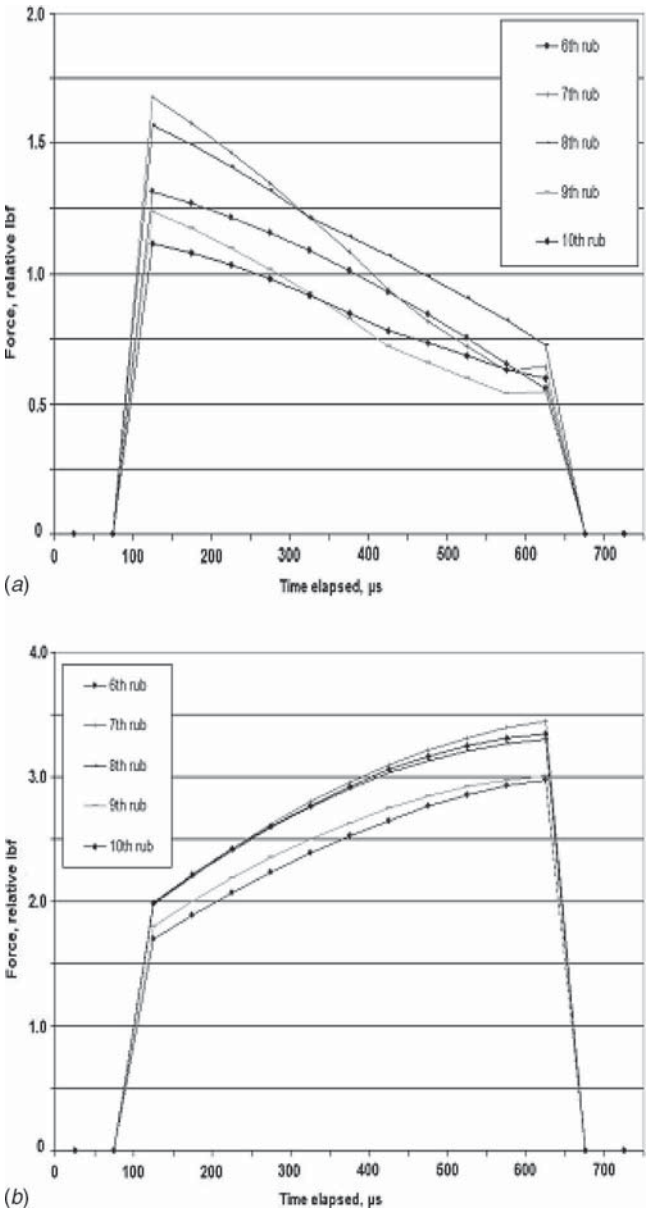

Fig. 17 (*a*) Axial component of tip force on airfoil in experiment no. 30. Incursion: ε=406 μm (0.0160 in.). (*b*) Circumferential component of tip force in experiment no. 30. Incursion: ε=406 μm (0.0160 in.).

In Table 1, five mode shapes are listed: first flex (1F), first torsion (1T), first and second compounds (C1, C2), and second flex (2F). Six strain gauges on the airfoil, i.e., three on the suction side and three on the pressure side, are then listed as an example. Their approximate location on the airfoil is reflected by their label as mid-chord at the airfoil tip (Tip M), trailing edge at the airfoil tip (Tip TE), mid-chord at the airfoil root (Root), leading edge at the airfoil tip (Tip LE), trailing edge at mid-span of the airfoil (TE M), leading edge at mid-span of the airfoil (LE M). The response level of each gauge location for each mode is then shown as percent of maximum value detected at the specific excitation frequency.

To quantify the effect of rub events, the measurements obtained from the OSU experiments were reduced to represent the stress of a particular gauge for a specified blade/casing interaction. Spectral analysis was applied to examine changes in frequency peak location and stress levels in selected frequency sub-domains. Knowledge of the natural frequencies of the blade provided an initial framework in order to isolate specific magnitudes of the power spectral density. This was then used to assess the possibility of severe stress occurring at each significant frequency.

A method of expediting the analysis of the data was conceived to ensure investigation of the appropriate segments of the signal for many different blade strikes. Naturally, the strikes were first grouped into the three main categories: advancing casing, zero-lead, and retreating casing. Only zero-lead rubs will be discussed in the following paragraphs.

For the purposes of creating frequency sub-domains for the spectral analysis, a number of possible filters were considered. A Chebychev II filter was finally selected. This filter allowed for a quick transition from the passband to the stopband region without ripples in the passband. Since the frequencies within the passband region represented information of the blade/engine casing contact, distortion of the response due to ripples was unacceptable. Ripples in the stopband region were permitted to exist however, as only

Table 1 Pre-experiment natural frequency responses

	Gauge	1 F 1.4 kHz	1 T 4 kHz	C1 4.7 kHz	C2 5.4 kHz	2 F 6.9 kHz
Suction Side	Tip M	1	−13	18	22	18
	Tip TE	1	7	−2	9	11
	Root	−100	100	4	62	88
Pressure Side	Tip LE	0	−17	8	3	0
	TE M	47	−67	100	20	−7
	LE M	23	7	24	100	100

the frequency content within the passband parameter was of importance. The choice of a specific filter method allowed for the creation of frequency sub-domains by lowpass, highpass, and bandpass variations of the Chebychev type II filter. These distinctions represented the frequencies that were allowed to pass unaltered in the passband region.

Following the above step, the bandpass filter was used to separate specific frequency ranges of the PSD in two manners: line and bin analyses. For a frequency line filter, the passband parameter was specified to only allow for a very small amount of frequencies to pass unaltered (a ±37 Hz range about the target frequency), while the bin filter extended the total passband range to the mid-interval point based on the data of Table 1. Finally, multiple bandpass filters incorporating these methods were used in succession to isolate the magnitude of the response about the targeted natural frequency.

An example of the final results for rub-induced stress deviations during zero-lead rubs is given in Figs. 18 and 19. The bin-filtered responses were used here based on the ability to more precisely identify the maximum response about the specified natural frequency.

The minimum, maximum and average normalized response is shown in Fig. 18 for the mid-chord root gauge location from experiment no. 26, $\varepsilon = 140$ μm (0.0055 in.). The gauge had recorded the largest stress in the first flexural mode and in the first torsional mode while vibrating as a cantilever beam free at the tip. The same situation occurs while the airfoil vibrates as a cantilever beam rubbing at the tip: the largest stress (normalized as 100%) is incurred in the range centered around 1.4 kHz (first flex) and centered around 4 kHz (first torsion). However, the same root gauge location is stressed differently while rubbing the case than while vibrating freely in the frequency range of the first combined mode C1 (centered around 4.7 kHz). The range of stress deviation over all recorded strikes at that frequencies went from 140% to 203% of the highest stress location on the airfoil for the C1 mode shape, with the average deviation measured at 175%. The effect of rubs at other frequencies is also shown in Fig. 18.

Similar normalized responses from experiment no. 26 are plotted for two tip strain gauge locations in Figs. 19(*a*) and 19(*b*). It is important to note that the leading edge tip strain gauge indicates rub-induced stress deviation from rubs only at the highest fre-

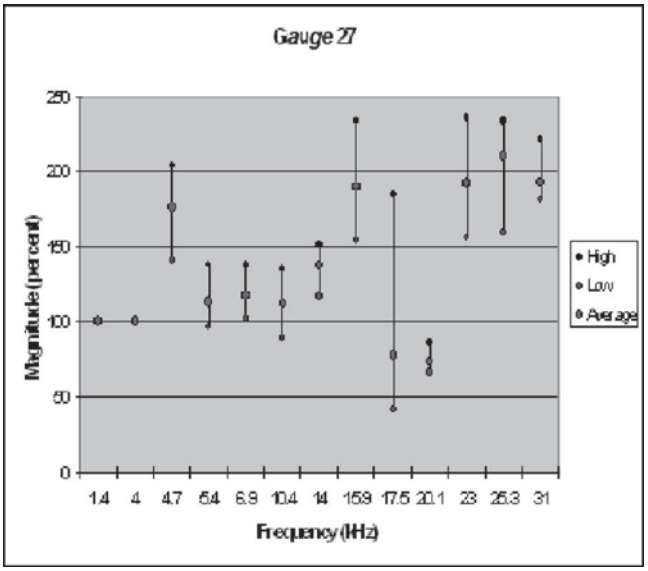

Fig. 18 Percent deviation of mid-chord root stresses on airfoil at selected frequencies

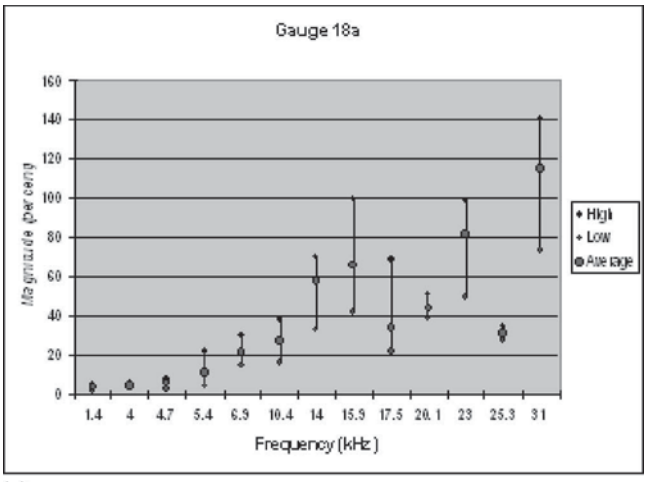

(*a*)

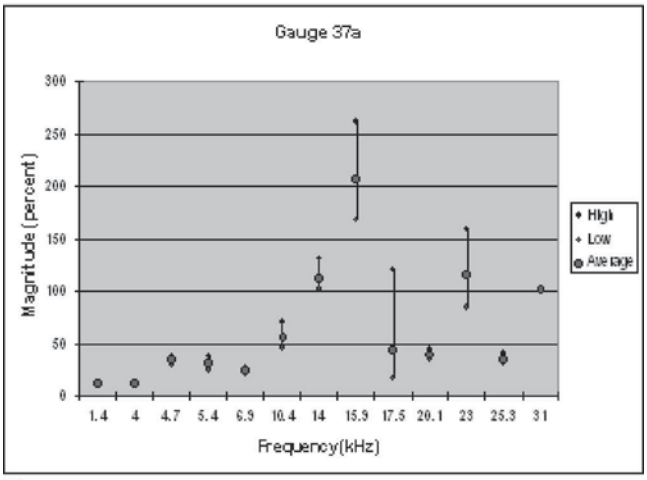

(*b*)

Fig. 19 (*a*) Percent deviation of LE tip stresses on airfoil at selected frequencies. (*b*) Percent deviation of TE tip stresses on airfoil at selected frequencies.

quency range, with a peak value measured at 141% of the highest stress location on the airfoil for the mode shape near 31 kHz. By contrast, the trailing edge tip gauge shows deviations in three of the modes above 11 kHz, with a peak value measured at 261% of the highest stress location on the airfoil for the mode shape near 16.9 kHz. It is conceivable that these levels of rub-induced stress deviation, when sustained over many more cycles than experienced in this experiment, could lead to substantial local damage. The results above would suggest a failure occurring first at the airfoil trailing edge as more likely.

In general, Figs. 18 and 19 are representative of results obtained for each individual strain gauge location for each experiment. They provide initial design guidelines regarding significant changes in blade dynamics during rub events.

In aggregate, the results discussed in this section begin to describe complete transients involving multiple successive incursions, tracking the blade tip contact force distribution and blade stresses throughout the observed rub event time frame, including blade motion during, between, and after successive casing strikes.

5 Conclusions

An in-ground spin-pit facility specifically designed to investigate aeromechanic phenomena for gas turbine engine hardware rotating at engine speed is presently in full operation at the OSU Gas Turbine Laboratory. An engine compressor disk, engine airfoil, and associated casing were used to obtain the blade/casing interaction experiments reported in this paper. The experiments were designed to obtain specific information related to prediction and modeling of blade-casing interactions.

The results presented describe the transient dynamics of rotor and casing vibro-impact response when an Inconel airfoil strikes a bare metal casing for several successive times under operational conditions similar to those experienced in flight. Sudden incursions of varying severity, defined by incursion depths ranging from 13 μm to 762 μm (0.0005 in. to 0.030 in.), were obtained. Tip loads and vibratory stresses occurring in rub events representative of in-flight events including a few rubs of varying incursion depth and positive or negative incursion rate and a few rubs at zero incursion rate have been demonstrated. In addition, the amplification of blade oscillations under successive rubs was obtained. The results discussed in this paper have been applied to advance the understanding of the complex physics of the rub phenomena and to compare the measurements to analytical predictions.

Acknowledgment

The work described in this paper was performed as part of the General Electric University Strategic Alliance program at The Ohio State University. Several GE engineers are contributing valuable research directions and assistance to the tip rub project. The authors wish to especially acknowledge the contributions of Kevin Turner, Dennis Corbly, Jim Rhoda, Alan Turner, A. J. Wang, and Sunil Sinha. We also would like to acknowledge the contributions to this work of Professor Maurice Adams of Case Western Reserve University and Dr. Michael Adams of Machinery Vibrations, Inc.

References

[1] Hermanek, F. J., Jr., 1970, "Coatings Lengthen Jet Engine Life," Metal Progress, **97**, pp. 104–106.

[2] Kosing, O. E., Scharl, R., and Schmuhl, H. J., 2001, "Design Improvements of the EJ 200 HP Compressor. From Design Verification Engine to a Future All Blisk Version," ASME Paper No. 2001-GT-0283.

[3] Sinha, S. K., 2005, "Non-linear Dynamic Response of a Rotating Radial Timoshenko Beam with Periodic Pulse Loading at the Free-end," Int. J. Non-Linear Mech., **40**(1), pp. 113–149.

[4] Turner, K., Adams, M.L., and Dunn, M.G., 2005, "Simulation of Engine Blade Tip-Rub Induced Vibration," ASME Paper No. GT2005-68217.

[5] Muszynska, A., 1989, "Rotor-to-Stationary Element Rub-Related Vibration Phenomena in Rotating Machinery—Literature Survey," Shock Vib. Dig., **21**, pp. 3–11.

[6] Padovan, J., and Choy, F. K., 1987, "Nonlinear Dynamics of Rotor/Blade/Casing Interactions," ASME J. Turbomach., **109**, pp. 527–534.

[7] Adams, M. L., 2000, *Rotating Machinery Vibration. From Analysis to Troubleshooting*, Marcel Dekker Inc., New York.

[8] Manwaring, S. R., and Wisler, D. C., 1993, "Unsteady Aerodynamics and Gust Response in Compressors and Turbines," ASME J. Turbomach., **115**, pp. 724–733.

[9] Kielb, J. J., Abhari, R. S., and Dunn, M. G., 2001, "Experimental and Numerical Study of Forced Response in a Full-Scale Rotating Turbine," ASME Paper No. 2001-GT-0263.

[10] Laverty, W. F., 1981, "Rub Energetics of Compressor Blade Tip Seals," *Proceedings of the 3rd International Conference on Wear of Materials*, pp. 714–721.

[11] Padova, C., Barton, J., Dunn, M. G., Manwaring, S., Young, G., Adams, M. L., and Adams, M., 2004, "Development of an Experimental Capability to Produce Controlled Blade Tip/Shroud Rubs at Engine Speed," ASME Paper No. GT2004-53322.

[12] Jiang, J., Ahrens, J., Ulbrich, H., and Scheideler, E. M., 1998, "A Contact Model of a Rotating Rubbing Blade," *Proceedings of the 5th International Conference on Rotor Dynamics*, Darmstadt, pp. 478–489.

[13] Ahrens, J., Ulbrich, H., and Ahaus, G., 2000, "Measurement of Contact Forces During Blade Rubbing," *Vibrations in Rotating Machinery*, 7th International Conference, Nottingham, September 12-14, ImechE, London, pp. 259–263.